Thermoviscoplastic Analysis of Hypersonic Structures Subjected to Severe Aerodynamic Heating

Earl A. Thornton* and J. Tinsley Oden†
University of Texas at Austin, Austin, Texas 78712
and
W. Woytek Tworzydlo‡ and Sung-Kie Youn§
Computational Mechanics Company, Inc., Austin, Texas 78752

A thermoviscoplastic computational method for hypersonic structures is presented. The method employs a unified viscoplastic constitutive model implemented in a finite element approach for quasistatic thermal-structural analysis. Applications of the approach to convectively cooled hypersonic structures illustrate the effectiveness of the approach and provide insight into the transient inelastic structural behavior at elevated temperatures.

Introduction

THE commitment to develop the National Aerospace Plane has generated resurgent interest in the technology required to design structures for hypersonic flight. Such structures will be exposed to aerodynamic heating of unprecedented magnitudes. As the vehicle accelerates or decelerates at hypersonic speeds in the atmosphere, shocks will sweep across the vehicle and interact with local shocks and boundary layers. These interactions introduce severe local pressures and heating rates. A recent experimental study[1] of interacting shock waves on a cylindrical leading edge shows heating rates 10 times undisturbed levels.

Leading edges of engine structures present a significant design problem because of intense local heating and pressures. Analysis of the flow shows that thermal and structural behavior present serious computational challenges to analysts because of the inherent nonlinearities in all aspects of the multidisciplinary problems. Some of the critical computational issues are identified in Ref. 2. Critical issues include the difficulties involved in 1) analyzing the viscous, compressible flow and predicting the high local aerodynamic heating; 2) modeling and analyzing multimode unsteady heat transfer in a high temperature convectively cooled structure; and 3) simulating the transient, nonlinear thermal-structural response for rapid temperature changes. Preliminary structural analysis of an impingement cooled leading edge[3] showed high local plasticity that seriously degraded the structure's load carrying capacity at elevated temperatures. A recent thermostructural analysis with experimental verification[4] of cowl lip designs confirmed that inelastic effects occur and can be significant. In the experimental study, two specimens failed due to burn through because of intense local heating or because of loss of cooling.

The purpose of this paper is to present a thermoviscoplastic computational method for hypersonic structures subjected to severe local unsteady heating. The analysis employs a unified viscoplastic constitutive model implemented in a finite element approach capable of predicting rate-dependent plasticity effects for temperatures up to about 75% of the melting point. Rate-dependent plasticity effects are known to be important at elevated temperatures.

Unified viscoplastic constitutive models have evolved over the last 20 years to provide a means for analytically representing a materials response from the elastic through the plastic range, including strain-rate dependent plastic flow, creep, and stress relaxation. The theories are guided by physical considerations including dislocation dynamics and are based on the principles of continuum mechanics. The first multidimensional formulations of elastic-viscoplastic constitutive equations was due to Bodner and Partom. Since then, a number of constitutive models have appeared; many of these theories are summarized in review articles that appear in Ref. 5. A NASA Lewis Research Center sponsored research program (HOST) conducted by the Southwest Research Institute recently concluded a four year research effort[6,7] to further develop unified constitutive models for isotropic materials and to demonstrate their usefulness for analysis of high temperature gas turbine engines. One result of this study is material property data for high temperature nickel-based alloys over a wide temperature range. The unified models employed were those of Bodner-Partom and Walker.

Unified viscoplastic theories have been implemented by a number of finite element researchers. The first use of unified constitutive models in a finite element program was by Newman et al.[8] Later, under the NASA HOST program, the Bodner-Partom and Walker models were implemented into finite element codes by General Electric and Pratt & Whitney. Kaufman et al.[9] describes these efforts as applied to gas turbine components. Moreno and Jordan[10] under the NASA HOST program developed and applied a unified constitutive model to gas turbine combustors using the MARC code. Detailed studies of several rate-dependent plasticity models and their numerical implementation using adaptive finite element methods were conducted by Bass[11] and Bass and Oden.[12,13] In another recent finite element application,[14] the Bodner-Partom and Walker theories were compared for a thin circular plate subject to highly localized, transient heating.

In this paper, the Bodner-Partom constitutive model is employed and the finite element approach developed in Refs. 11-13 for the isothermal case is extended to include thermal effects. The paper begins by describing the finite element approach used for thermal analysis of convectively cooled hypersonic structures. Then the thermoviscoplastic structural analysis is presented. The initial value problem is formulated, the constitutive model is described, and the finite element viscoplastic solution method is presented. Next, applications of the approach are made to convectively cooled structures.

Presented as Paper 89-1226 at the AIAA/ASME/ASCE/AHS/ASC 30th Structures, Structural Dynamics, and Materials Conference, Mobile, AL, April 3-5, 1989; received May 6, 1989; revision received Feb. 1, 1990.

*Visiting Scholar, Texas Institute of Computational Mechanics; currently at Department of Mechanical and Aerospace Engineering, University of Virginia, Charlottesville, VA 22901. Associate Fellow AIAA.
†Director, Texas Institute of Computational Mechanics.
‡Senior Research Engineer.
§Senior Research Engineer.

An appendix presents thermal and structural data for the convectively cooled hypersonic structure used in the numerical computations.

Thermal Analysis of Hypersonic Structures

Convectively cooled structures are strong candidates for use in hypersonic flight vehicles. For hypersonic flight, some leading edges and panels require active cooling systems to keep structural temperatures within acceptable ranges. The internal flow in the coolant passage has a predominant role in the thermal response of a hypersonic structure subject to external heating. A cross section of a typical convectively cooled structure is shown in Fig. 1. An aerodynamic skin and a coolant passage with internal heat exchanger protect the primary structure from the aerodynamic heating. The thin, typically metallic aerodynamic skin transfers the energy of the aerodynamic heating to a low-temperature coolant flow through the heat exchanger fins that connect the aerodynamic skin to the primary structure. In a typical engine structure, the coolant is cold hydrogen that later is used as the propulsion system fuel.

Heat transfer in the aerodynamic skin consists of conduction combined with surface radiation. Heat transfer between the aerodynamic skin, the heat exchanger surfaces, and the primary structure is by conduction at the solid-fluid interface. The finite element representation of conduction heat transfer with radiation boundary conditions follows the standard procedures described in Ref. 15.

The dominant mode of heat transfer in the coolant flow is forced convection. The representation of the heat transfer in the coolant passage is the critical step in the heat transfer analysis. There are two basic representations that can be employed. The first, denoted here as the engineering model, is based on a number of assumptions that greatly simplify the problem into a single energy equation with a specified mass flow rate. Detailed computation of the fluid velocity components and temperatures is not required. The second representation idealizes the coolant flow as a continuum model, and the partial differential equations describing conservation of mass, momentum, and energy are solved simultaneously to obtain fluid velocity and temperature distributions. This latter model is the most accurate, but it is also considerably more expensive than the engineering model. In this paper, the engineering heat-transfer model is employed.

Engineering Model for Coolant Passages

The basic features of the engineering model are developed from the idealization shown in Fig. 2. A segment of the coolant passage of width w is shown; for simplicity, only the upper one-half of the coolant passage with the aerodynamic skin is shown. The engineering formulation[16] is based on the following assumptions:

1) The thermal energy state of the fluid is characterized by the fluid bulk temperature T_F, which varies only in the flow direction, i.e., $T_F(x,t)$.

2) The flow is represented by the mass flow rate $\dot{m}$ in the coolant passage specified by $\dot{m}=\rho_F A_F V_F$, where ρ_F is the passage, and V_F the coolant mean flow velocity.

3) A convection coefficient h is defined such that the heat flux $\dot{q}_F$ transferred between the structure and the coolant may be expressed as

$$\dot{q}_F = h(T_S - T_F)$$

where $T_S(x,t)$ denotes the structural temperature at the fluid-solid interface.

4) The convection coefficient h may be expressed as a function of the fluid bulk temperature alone by using analytical/empirical equations for the Nusselt number,

$$Nu = hD/k_F$$

where D is the hydraulic diameter of the coolant passage and k_F the thermal conductivity of the fluid coolant. The convection coefficient as well as the solid and fluid thermal parameters may, in general, be temperature dependent.

With these assumptions, energy balances on the aerodynamic skin and coolant give the governing conservation equations.

Fluid:

$$-\frac{\partial}{\partial x}k_F A_F \frac{\partial T_F}{\partial x} - wh(T_S - T_F) + \dot{m}c_F \frac{\partial T_F}{\partial x} + \rho_F c_F A_F \frac{\partial T_F}{\partial t} = 0 \tag{1}$$

Solid:

$$-\frac{\partial}{\partial x}k_S A_S \frac{\partial T_S}{\partial x} + wh(T_S - T_F) + \sigma\epsilon T^4 + \rho_S c_S A_S \frac{\partial T_S}{\partial t} = \dot{q} \tag{2}$$

where the subscripts F and S denote the fluid and solid, respectively. In these equations, c denotes specific heat, σ is the Stefan-Boltzmann constant, and ϵ the surface emissivity. Because of the temperature dependence of the thermal parameters and the radiation term, Eqs. (1) and (2) constitute a nonlinear set of partial differential equations.

The heat exchanger fins are not included explicitly in this model. However, the heat transfer between the heat exchanger fins and coolant approximately can be taken into consideration through the use of an effective width w, which represents the area over which the convective heat exchange occurs.

Finite Element Formulation for Coolant Passages

A typical finite element representing Eqs. (1) and (2) is characterized by fluid and fluid-solid interface nodes. The element shown in Fig. 3 has two fluid nodes (I and J) and two fluid-solid interface nodes (K and L). Within the element, the

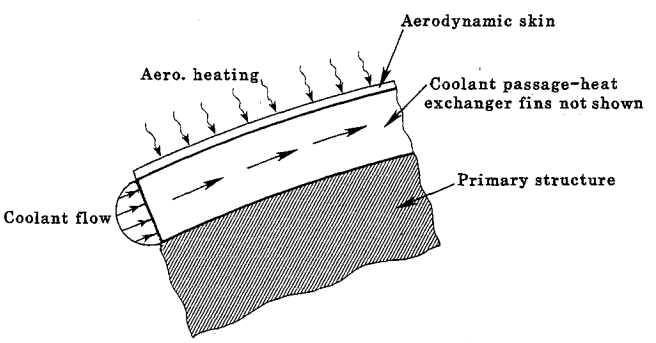

Fig. 1 Convectively cooled structure.

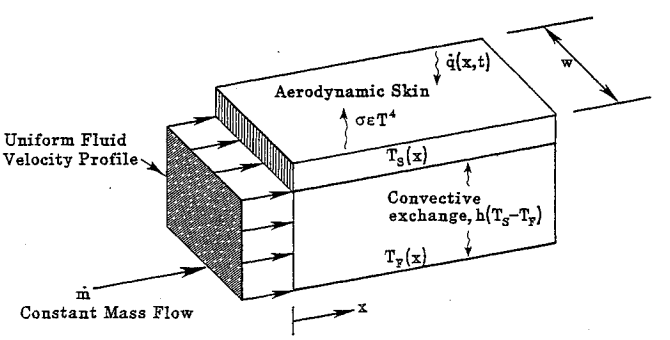

Fig. 2 Engineering model of coolant passage heat transfer.

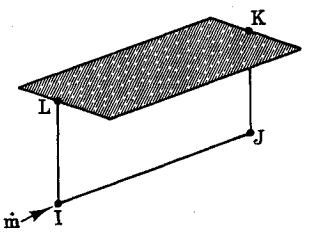

Fig. 3 Finite element model of coolant passage.

fluid and solid temperatures are expressed as

$$T_F = [N(x)]\{T_F\} \tag{3a}$$

$$T_S = [N(x)]\{T_S\} \tag{3b}$$

where $[N(x)]$ are the element interpolation functions. Following usual finite element procedures,[15] the discretized equations for an element of length L may be derived in the form

$$\begin{bmatrix} C_F & 0 \\ 0 & C_S \end{bmatrix} \begin{Bmatrix} \dot{T}_F \\ \dot{T}_S \end{Bmatrix} + \begin{bmatrix} K_v + K_h + K_F & -K_h \\ -K_h & K_S + K_R \end{bmatrix} \begin{Bmatrix} T_F \\ T_S \end{Bmatrix} = \begin{Bmatrix} 0 \\ Q \end{Bmatrix} \tag{4}$$

where the element capacitance matrices are given by

$$[C_F] = \int_o^L \rho_F c_F A_F \{N\}[N]\, dx \tag{5a}$$

$$[C_S] = \int_o^L \rho_S c_S A_s \{N\}[N]\, dx \tag{5b}$$

and the element conductance matrices are

$$[K_v] = \int_o^L \dot{m} c_F \{N\}\left[\frac{dN}{dx}\right] dx \tag{6a}$$

$$[K_h] = \int_o^L wh\{N\}[N]\, dx \tag{6b}$$

$$[K_F] = \int_o^L k_F A_F \left\{\frac{dN}{dx}\right\}\left[\frac{dN}{dx}\right] dx \tag{6c}$$

$$[K_S] = \int_o^L k_S A_S \left\{\frac{dN}{dx}\right\}\left[\frac{dN}{dx}\right] dx \tag{6d}$$

$$[K_R]\{T_S\} = \int_o^L \sigma \epsilon T^4 \{N\}\, dx \tag{6e}$$

The element equations given in Eq. (4) show that the coolant passage model can be regarded as an assembly of elements where each element represents a single heat transfer mode. Thus, we can represent the coolant passage in terms of two convective elements: 1) a mass-transport element, and 2) a surface convection element. The mass-transport element represents the downstream convective heat transfer due to mass flow; it has a capacitance matrix $[C_F]$ as well as conductance matrices $[K_v]$ and $[K_F]$. The surface convection element represents the convection heat exchange between the coolant fluid and the solid; it does not have a capacitance matrix, but it has a conductance matrix $[K_h]$ linking the solid and fluid nodes. These coolant passage elements are assembled into the finite element thermal model for the complete convectively cooled structure that has conduction elements, radiation elements, and surface elements for convection to a specified convective exchange temperature.

The unsteady thermal analysis is nonlinear because of temperature-dependent thermal properties and surface radiation. The equations are solved by time marching with the Crank-Nicolson algorithm; at each time step, the nonlinear algebraic equations are solved by Newton-Raphson iteration.

Thermoviscoplastic Structural Analysis

The behavior of a thermoviscoplastic structure subjected to aerodynamic heating is analyzed assuming that: 1) thermomechanical coupling in the conservation of energy equation can be neglected, 2) the structural response is quasistatic, and 3) deformations are infinitesimal. With these assumptions, an unsteady thermal analysis may be performed first to determine the temperatures. Then, using these temperatures, the structure's viscoplastic response is determined. The solution is thus obtained by separately solving initial boundary value problems for first the thermal and then the structural response.

Initial Value Viscoplasticity Problem

Consider a viscoplastic structure occupying a region Ω with boundary $\partial\Omega$. The behavior of the structure is described by the following system of differential equations.

Equilibrium in rate form:

$$\dot{\sigma}_{ij,j} + \dot{b}_i = 0 \tag{7}$$

where σ_{ij} denote components of the stress tensor, b_i are the body force components per unit volume, and the summation convention is employed.

Kinematic relation for velocity gradients:

$$\dot{\epsilon}_{ij} = \dot{\epsilon}^E_{ij} + \dot{\epsilon}^P_{ij} = (\dot{u}_{i,j} + \dot{u}_{j,i})/2 \tag{8}$$

where ϵ_{ij} denotes the total strain components and superscripts E and P denote elastic and inelastic strain components, respectively. The components of the displacement rates are $\dot{u}_i$.

Constitutive relations:

$$\dot{\sigma}_{ij} = E_{ijkl}\dot{\epsilon}^E_{kl} - E_{ijkl}\alpha_{kl}\Delta\dot{T} \tag{9a}$$

$$\dot{\epsilon}^P_{ij} = f_{ij}(\sigma_{ij}, Z_k) \qquad \text{(no sum)} \tag{9b}$$

$$\dot{Z}_i = g_i(\sigma_{ij}, Z_k) \qquad \text{(no sum)} \tag{9c}$$

where E_{ijkl} represent Hooke's tensor of elasticity parameters, α_{kl} are components of a tensor of thermal expansion parameters, and ΔT represents the rate of the change in temperature. Both E_{ijkl} and α_{kl} are temperature dependent. The constitutive functions are f_{ij} and g_i where Z_k represents internal state variables. These functions and state variables characterize the viscoplastic response of the material.

The description of the problem is completed by prescribing the boundary and initial conditions,

$$\dot{u} = \dot{\bar{u}}_i \text{ on } \partial\Omega_1 \tag{10a}$$

$$\dot{\sigma}_{ij} n_j = \dot{\bar{\sigma}}_i \text{ on } \partial\Omega_2 \tag{10b}$$

where $\dot{\bar{u}}_i$ are prescribed surface displacement rates, n_j the components of a unit normal vector, and $\dot{\bar{\sigma}}_i$ the prescribed surface traction rates. The initial conditions include specifying the displacements, stresses, and internal state variables, i.e.,

$$u_i(x,0), \sigma_{ij}(x,0), Z_i(x,0)\ x \epsilon \Omega$$

Constitutive Model

The Bodner-Partom constitutive model is of the internal state variable type that is based on phenomenological observa-

tions and supported by physical concepts related to dislocation dynamics. The model has gone through several modifications and was extended for anisotropic work hardening materials. The current model[5,6] also includes temperature effects.

Flow Law

For the inelastic strain rate component, the isotropic form of the Prandtl-Reuss law is assumed

$$\dot{\epsilon}_{ij}^P = \lambda S_{ij} \tag{11a}$$

$$\dot{\epsilon}_{kk}^P = 0 \qquad \lambda > 0 \tag{11b}$$

where S_{ij} are the deviatoric stress components given by

$$S_{ij} = \sigma_{ij} - (1/3)\delta_{ij}\sigma_{kk} \tag{12}$$

and $\dot{\epsilon}_{kk}^P = 0$ denotes plastic incompressibility.

Kinematic Equation

Squaring Eqs. (11) leads to

$$\lambda^2 = D_2^P / J_2 \tag{13}$$

where D_2^P and J_2 are the second invariants of the strain rate and stress tensors, respectively. For example, the deviatoric stress invariant is

$$J_2 = (1/2)S_{ij}S_{ij} \tag{14}$$

The relation governing inelastic deformations is the kinetic equation, and the form taken by Bodner-Partom is

$$D_2^P = D_0^2 \exp[-(Z^2/3J_2)^n] \tag{15}$$

where D_0 is the limiting strain rate in shear, n is a temperature-dependent material parameter, and Z is interpreted as a load history dependent parameter (herein called the internal state variable) that represents the hardness of the material with respect to resistance to plastic flow. Combining Eqs. (11–13) gives

$$\dot{\epsilon}_{ij}^P = (S_{ij}/\sqrt{J_2})D_0 \exp\left[-(1/2)(Z^2/3J_2)^n\right] \tag{16}$$

Evolution Equations of Internal State Variable

The internal state variable Z consists of isotropic and directional components,

$$Z = Z^I + Z^D \tag{17}$$

The evolution equation proposed for the isotropic hardening component[5] is

$$\dot{Z}^I(t) = m_1[Z_1 - Z^I(t)]\dot{W}_p(t) - A_1 Z_1\left[\frac{Z^I(t) - Z_2}{Z_1}\right]^{r_1} \tag{18}$$

with the initial condition, $Z^I(0) = Z_0$. In the first term, Z_1 is the limiting (saturation) value of Z^I, m_1 is the hardening rate, and the plastic work rate is

$$\dot{W}_p = \sigma_{ij}\dot{\epsilon}_{ij}^P \tag{19}$$

which is taken as the measure of hardening. Z_2 is the minimum value of Z^I at a given temperature, and A_1 and r_1 are temperature dependent material constants.

The evolution form of the directional hardening component[5] is defined as

$$Z^D(t) = \beta_{ij}(t)u_{ij}(t) \tag{20}$$

where u_{ij} are the direction cosines of the current stress state,

$$u_{ij} = \sigma_{ij}(t)/[\sigma_{kl}(t)\sigma_{kl}(t)]^{1/2} \tag{21}$$

The evolution equation for $\beta_{ij}(t)$ has the same general form as that for isotropic hardening but has tensorial character,

$$\dot{\beta}_{ij}(t) = m_2[Z_3 u_{ij}(t) - \beta_{ij}(t)]\dot{W}_p(t) - A_2 Z_1\left\{\frac{[\beta_{kl}(t)\beta_{kl}(t)]^{1/2}}{Z_1}\right\}^{r_2} v_{ij}(t) \tag{22}$$

where

$$v_{ij}(t) = \beta_{ij}(t)/[\beta_{kl}(t)B_{RL}(t)]^{1/2} \tag{23}$$

$$\beta_{ij}(0) = 0 \tag{24}$$

As in Eq. (18), m_2 is the hardening rate. A_2 and r_2 are temperature-dependent material constants. Other variants of the isotropic and directional hardening variables are described in Refs. 5–7. There references also present data for the parameters used in constitutive models for several materials. The particular values used in the present study are presented in the Appendix.

Finite Element Formulation

The finite element formulation follows the approach of Ref. 11, and the details of the weak formulation are presented there. Since the approach presented in Ref. 11 is for the isothermal case, this formulation extends the previous approach by the inclusion of temperature effects.

The finite element approach approximates displacement rates within an element by taking the displacement rates as

$$\{\dot{u}\} = [N]\{\dot{\delta}\} \tag{25}$$

where $[N]$ are the interpolation functions and $\{\dot{\delta}\}$ represent the nodal displacement rates. Using the strain-displacement equations in rate form, Eq. 8, an element's strain rates can be computed as

$$\{\dot{\epsilon}\} = [B]\{\dot{\delta}\} \tag{26}$$

where $[B]$ is the strain-displacement matrix. Following usual finite element procedures, the finite element equations for a typical element are,

$$[K(T)]\{\dot{\delta}\} = \{\dot{F}_p\} + \{\dot{F}_T\} + \{\dot{F}_\sigma\} + \{\dot{F}_B\} \tag{27}$$

where $[K(T)]$ is the element stiffness matrix, and the terms on the right side are element load vectors due to the rate of plastic strains, temperature, surface tractions and body forces, respectively. These matrices are defined by

$$[K(T)] = \int_{\Omega e} [B]^T[E(T)][B]\, d\Omega \tag{28}$$

$$\{\dot{F}_p\} = \int_{\Omega e} [B]^T[E(T)]\{\dot{\epsilon}^p\}\, d\Omega \tag{29}$$

$$\{\dot{F}_T\} = \int_{\Omega e} [B]^T[E(T)]\{\alpha(T)\}\Delta\dot{T}\, d\Omega \tag{30}$$

$$\{\dot{F}_{\bar{\sigma}}\} = \int_{\partial\Omega e} [N]^T\{\dot{\bar{\sigma}}\}\, ds \tag{31}$$

$$\{\dot{F}_B\} = \int_{\Omega e} [N]^T\{\dot{b}\}\, d\Omega \tag{32}$$

where Ω_e denotes the element volume, and $\partial\Omega_e$ denotes an element surface where tractions are defined.

The temperature affects the viscoplastic structural analysis directly in three ways: 1) the elasticity matrix $[E(T)]$ and the coefficients of thermal expansion $\{\alpha(T)\}$ depend on tempera-

ture, 2) nodal loads $\{\dot{F}_T\}$ depend on the local temperature rates, and 3) several parameters in the Bodner-Partom constitutive model are temperature dependent.

Viscoplastic Solution Method

Since the present approach uses an uncoupled (sometimes called one-way coupled) formulation, the thermal problem is solved first followed by the viscoplastic analysis. The transient thermal problem is solved by time marching with a time step Δt_T, and the nodal temperatures at successive times $t_1, t_2, \ldots$ are obtained. These temperature vectors are used as input to the structural analysis.

The first computation in the structural analysis is to solve an initial statics problem if the initial temperature distribution $T(x,0)$ is not equal to a uniform reference temperature or if any initial static loads are present. The results of this analysis are the initial conditions (displacements and stresses) for the transient viscoplastic analysis.

The viscoplastic analysis time marches with a time step Δt_s. Experience has shown that the time step required for the structural analysis is usually smaller than for the thermal analysis, i.e., $\Delta t_s < \Delta t_T$. At intermediate times in the structural analysis, the temperatures are linearly interpolated from the temperatures known at the beginning and end of the larger thermal time intervals.

The strategy employed in the viscoplastic algorithm is as follows: with the initial distribution of stress, temperature and internal variables specified use the equilibrium condition (Eq. 27) to obtain the nodal displacement rates. Then integrate the constitutive equations forward in time at the element Gauss integration points. With updated values of the stress, temperature and internal variables at the new time, the equilibrium equation is solved again. This sequence of determining the nodal displacement rates, then advancing the constitutive equations in time is continued until the desired history of the initial boundary-value problem has been obtained.

Thus, the algorithm proceeds through the following steps:

1) At time t, initialize σ_{ij}, Z_i for each element;
2) Calculate $\dot{\epsilon}^P_{ij} = f_{ij}(\sigma_{ij}, Z_k)$ for each element;
3) Assemble and solve $[K]\{\dot{\delta}\} = \{\dot{F}\}$;
4) Calculate $\dot{\epsilon}_{ij}$ for each element, $\{\dot{\epsilon}\} = [B]\{\dot{\delta}\}$;
5) Calculate $\dot{\sigma}_{ij}$ for each element, $\{\dot{\sigma}\} = [E]\{\dot{\epsilon} - \dot{\epsilon}^P\} - [E]\alpha\Delta\dot{T}$;
6) Calculate $\dot{Z}_i$ for each element, $\dot{Z}_i = g_i(\sigma_{ij}, Z_k)$;
7) Intergrate $\dot{\sigma}_{ij}$, $\dot{Z}$ forward for each element to get σ_{ij} and Z_i at $t + \Delta t_s$;
8) If $t + \Delta t_s < t_{\text{final}}$ go to 2, otherwise stop.

This computational method has been presented for a constant time step Δt_s. Computational experience by several investigators[7-14] indicates that a very small time step can be required because of the stiff nature of the ordinary differential equations describing the internal state variables. To gain improved efficiency and reliability a variable time step algorithm has been implemented.

Variable Time Step Algorithm

In the constant time step viscoplastic algorithm, the internal state variables are advanced in time with the conditionally stable Euler forward difference algorithm. The variable time step algorithm is a predictor-corrector scheme using a truncation error criterion[17] to adjust the time step.

For simplicity, consider the single ordinary differential equation,

$$\dot{y} = f(y,t) \tag{33}$$

The solution is advanced using a predictor-corrector scheme. The predictor phase consists of an Euler step:

$$y^P_{t+\Delta t} = y_t + \Delta t \dot{y}_t \tag{34}$$

$$\dot{y}^P_{t+\Delta t} = f(y^P_{t+\Delta t}, t + \Delta t) \tag{35}$$

An error indicator E[17] is then computed from

$$E = \frac{|\Delta t(\dot{y}^P_{t+\Delta t} - \dot{y}_t)|}{2|y^P_{t+\Delta t}|} \tag{36}$$

The error indicator is next compared with a preset error criterion, and, if the criterion is met, the time step is sufficiently small enough to proceed to the corrector stage. Otherwise, the predictor phase Eqs. (34) and (35) is repeated with a smaller time step. For the Bodner-Partom evolution equations the control variables used to calculate the error indicator were components of a stress tensor σ_{ij}, state variables Z_i, and plastic work W_p. This means that every single component of the stress tensor σ_{ij}, all state variables Z_i, and plastic work W_p were consecutively substituted for a generic variable y in Eq. (36), and then the maximum value of error was used for the time step evaluation. In most examples solved, the stress components or the plastic work actually controlled the time step.

The corrector phase is the modified Newton scheme,

$$\dot{y}_{\text{avg}} = (\dot{y}_t + \dot{y}^P_{t+\Delta t})/2 \tag{37}$$

$$\dot{y}^C_{t+\Delta t} = y_t + \Delta t \dot{y}_{\text{avg}} \tag{38}$$

A flow chart depicting the adaptive scheme is shown in Fig. 4. The flow chart shows how the time step is either reduced or increased depending on the error indicator, Eq. (36). The flow chart shows that the time step is reduced or increased by a factor of two. This approach is effective, but an alternate scheme also has been used where the new time step is based on the error E. In this scheme

$$\Delta t = \Delta t \sqrt{\frac{E_{\text{opt}}}{E}} \tag{39}$$

where $E_{\text{opt}} = \sqrt{E_{\max} E_{\min}}$. Error tolerances $E_{\max}$ and $E_{\min}$ are specified by the user, typical values being $E_{\max} = 0.05$ and $E_{\min} = 0.005$.

Applications

As mentioned in the Introduction, leading edges of engine structures can experience intense local heating due to shock interactions. Two models of such structures are analyzed for heat loads representative of shock interactions. Material properties used (see the appendix) represent a high-temperature nickel-based super alloy. Computations are performed first for a simplified one-dimensional model to provide insight into the computational procedure. Then a two-dimensional model of a realistic convectively cooled structure is analyzed in detail.

Simplified One-Dimensional Model

To gain a preliminary understanding of the behavior of a convectively cooled structure subjected to convective heating, a simple one-dimensional bar model was investigated. A segment (Fig. 5a) of the aerodynamic skin is modeled assuming uniform temperature. The coolant is assumed to have a constant, specified temperature, and the skin is heated convectively. A strong time variation of the convection coefficient (Fig. 5b) simulates the passage of a moving shock. The aerodynamic surface experiences an energy loss due to radiation assuming the surface emissivity has a value of 0.8. The resulting transient temperature and bar compressive stress exhibit features to be expected in a more complex model.

The transient temperature history (Fig. 6a) shows a rapid rise following the sudden increase in the convective coefficient and then a smooth decay after the large convective heating is removed. The convective cooling causes the temperature to return quickly to equilibrium. The initial rapid increase in temperature causes the bar to yield in compression very early in the response (Fig. 6b). After the temperature begins to

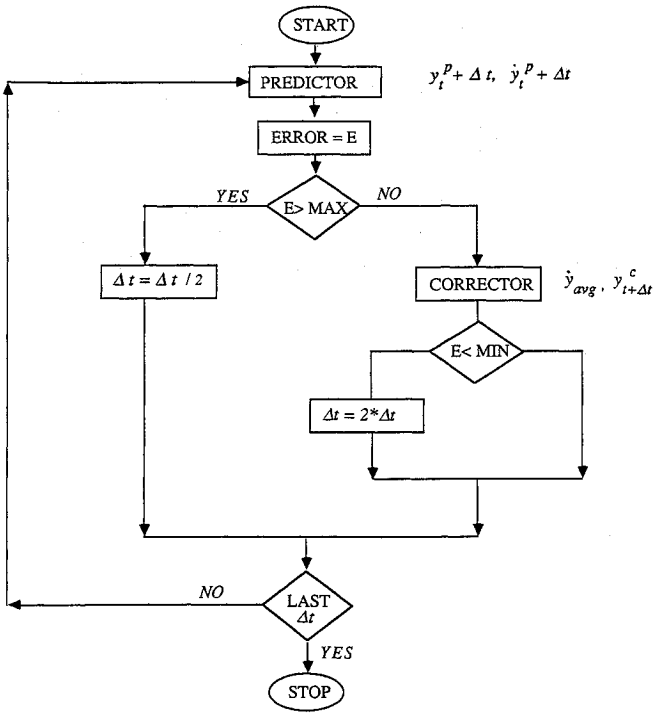

Fig. 4 Flow chart for adaptive time step algorithm.

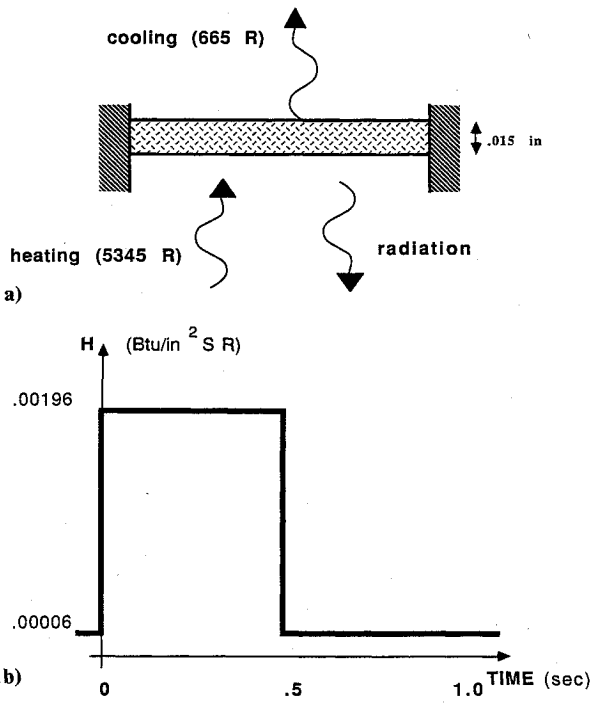

Fig. 5 One-dimensional model of convectively cooled structure: a) thermal-structural model; and b) convection coefficient history.

decay at $t = 0.5$ s, the stress rapidly changes to tension; hence, as the temperature returns to equilibrium a large residual tensile stress remains in the bar. The tensile stress is induced because the initial high temperature causes compressive yielding. This yielding tends to permanently shorten the bar. However, the bar's fixed end boundary conditions prohibit the bar from decreasing in length as the temperature decreases so that a tensile stress develops as the material cools.

To evaluate the effect of viscoplastic behavior, the same problem was solved assuming purely elastic properties of material (dashed line in Fig. 6b). As expected, neglecting viscoplasticity results in enormous compressive stresses due to heating and no residual stress.

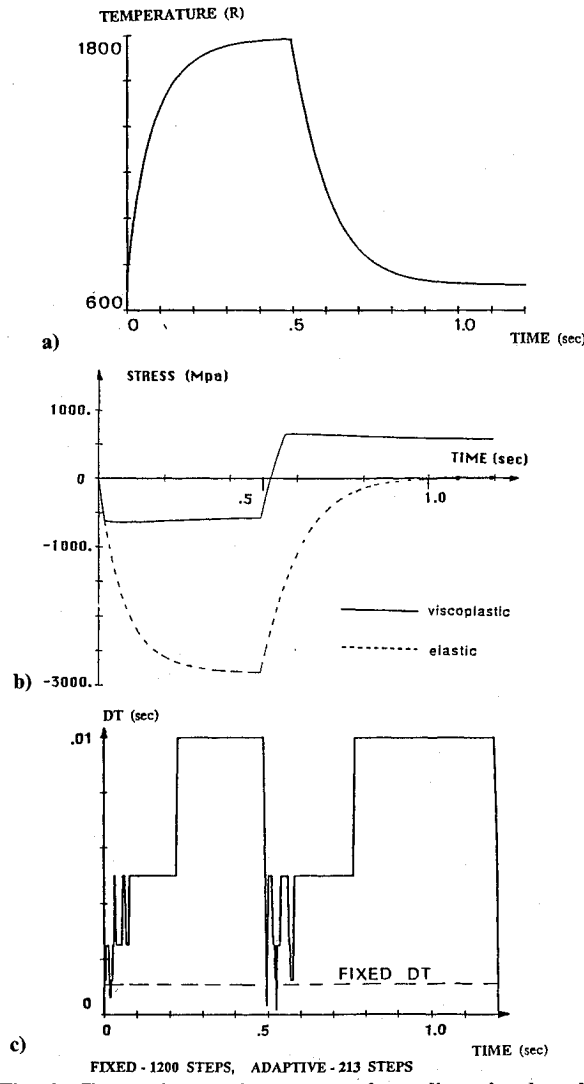

Fig. 6 Thermoviscoplastic response of one-dimensional model: a) temperature history; b) stress history; and c) adaptive time step history.

During the thermal-structural analyses, an uncertainty arose concerning applicability of the hardness evolution equation, Eq. (18), at high temperature rates (about 5000°C/s) occurring in these analyses. At such high-temperature rates this equation may predict somewhat anomalous behavior of the material. This is illustrated by the following example. Consider a specimen of superalloy B 1900 + Hf with properties presented in the appendix. If the virgin, load-free specimen is heated from 760°C to 1060°C in 0.1 s, the temperature-dependent variable Z_2 drops from 2700 to 1200 MPa. However, the actual hardness variable Z^1, which follows Z_2 only through the relatively slow thermal recovery term [second term in Eq. (18)] reduces in this time only to 2696 MPa. This means that although the specimen has reached an elevated temperature, it has not yet softened—a somewhat surprising result. The need for further research in thermal history effects on B 1900 + Hf was noted in Ref. 6.

In the initial viscoplastic analysis, a fixed time step of 0.001 s was used, and 1200 time steps were required for the analysis. The variable time step algorithm shown in Fig. 4 was then implemented and the problem was resolved. Figure 6c shows the history of the variable time step and indicates that the new analysis required only 213 steps. The figure shows that in the flat part of the stress response a large time step was used, but near $t = 0$ and again at $t = 0.5$ s, when the stress is changing rapidly, small time steps are needed to capture the response accurately. The actual reduction of the computational cost is smaller than the ratio of number of time steps.

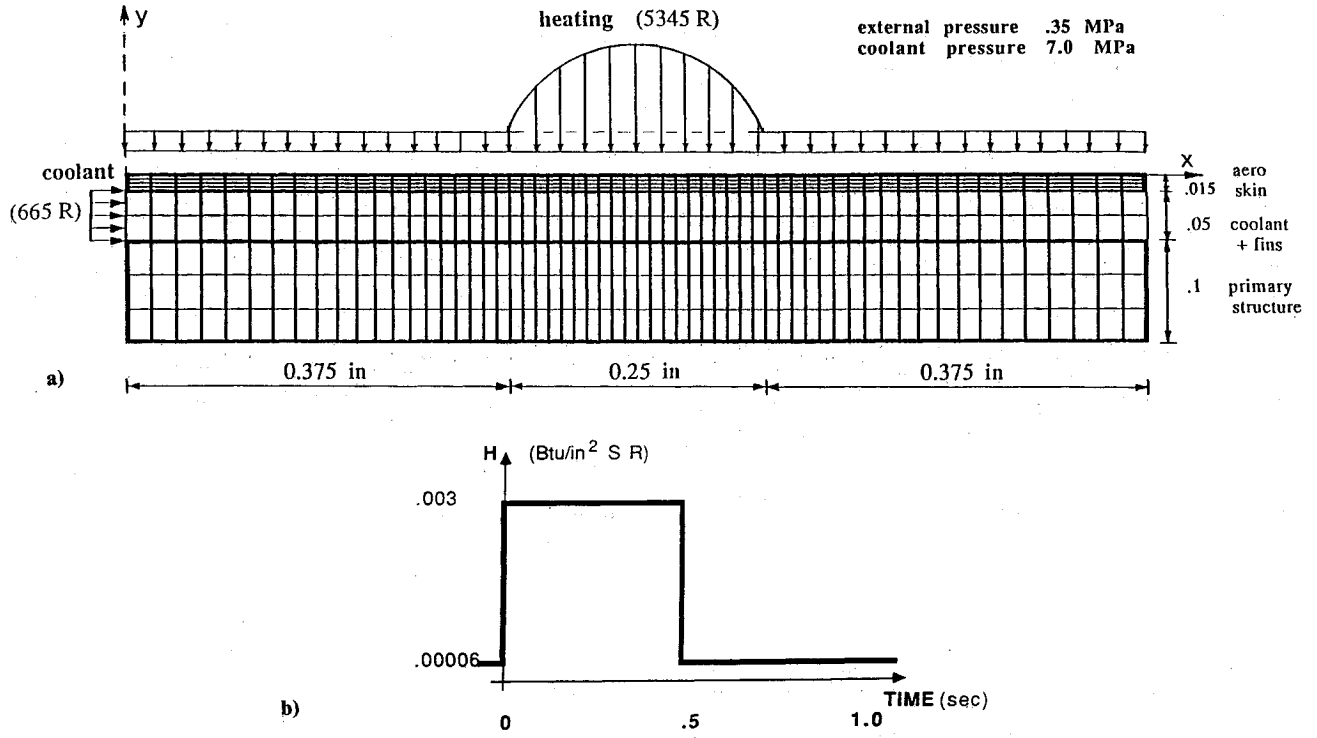

Fig. 7 Two-dimensional model of convectively cooled structure: a) thermal-structural model; and b) convection coefficient history.

This is caused by a higher cost of the predictor-corrector method (as compared with forward Euler) and the additional cost of error evaluation, time step adjustment, etc. In this particular example, the adaptive procedure reduced the total computation time by a factor of 0.45, with results obtained with both methods being practically the same (less than 1% difference). This example shows that the adaptive time step algorithm is an important step toward producing a reliable, accurate solution.

Convectively Cooled Structure

A more realistic two-dimensional model of a convectively cooled hypersonic structure is shown in Figs. 7. The model represents a segment of a convectively cooled structure such as a wall of a scramjet engine fuel injection strut. The finite element thermal model (Fig. 7a) includes: 1) conduction heat transfer in the aerodynamic skin, heat exchanger fins, and primary structure; 2) convective heat transfer between the walls of the coolant passage and coolant; 3) mass transport convection in the coolant, which has an unknown bulk temperature; and 4) surface radiation on the aerodynamic skin. The aerodynamic skin is uniformly convectively heated over its length, and superimposed on the uniform heating is a local, intense heating simulating a transient shock. The transient heating is induced by the time-dependent convection coefficient shown in Fig. 7b.

In the plane strain structural finite element model, the primary structure and aerodynamic skin have unit thickness, but the heat exchanger fins in the coolant passage are approximately represented by a single fin with the total thickness of 0.060 in. The wall segment has fixed displacement boundary conditions at the left and right ends. The aerodynamic skin, exchanger fins, and primary structure are also loaded by internal pressure (7.0 MPa = 1000 psi) in the coolant passage, which is relatively large compared to external aerodynamic pressure (0.35 MPa = 50 psi).

The model was analyzed first for steady aerodynamic heating and internal pressure operating conditions. Then the sudden localized aerodynamic heating was applied. Thus, the steady temperatures and stresses serve as initial conditions for the transient thermoviscoplastic analysis.

The viscoplastic solution was computed with the variable time step algorithm, and the time step was varied using Eq. (39). A total of 265 steps were required to compute the response for a total time duration of 1.2 s.

The thermal response of the wall segment is shown in Fig. 8. Figure 8a shows the time history of the temperature at a point on the aerodynamic skin directly under the transient heating. Figure 8b shows contours of temperatures at $t = 0.5$ s when temperatures are maximum. The temperature history is qualitatively similar to the results obtained in the one-dimensional model showing the rapid skin temperature rise and fall with the simulated shock heating. The temperature contours show relatively steep thermal gradients induced by the local heating, and that the coolant substantially limits the extent of the induced high temperatures. Thus the high temperatures are confined to the aerodynamic skin, and the primary structure experiences only small temperature changes. The temperature gradients in the skin, particularly at the coolant-skin interface, are not predicted with high accuracy because of the engineering model of the coolant heat transfer. However, local temperature levels in the skin are reasonably accurate since net energy transfer to the coolant is modeled satisfactorily.

Viscoplastic histories of the horizontal stress component σ_x at two points through the skin thickness ($x = 0.5$, $y = 0$, and $y = -0.0075$) are shown and compared with an elastic solution in Fig. 9. The stress histories follow the temperature and, under the intense local heating stresses, are very similar to the results obtained from the one-dimensional model. At this location, the skin yields through most of its thickness. After the heating ceases there is a rapid decay of stress, and under the intense local heating there are residual tensile stresses. Figure 10 shows the time history of the vertical component of stress σ_y in the heat exchanger fins ($x = 0.5$, $y = -0.04$). High tensile stresses are induced with significant local yielding that are followed by residual compressive stress. The crude finite element model of the fins only approximates these stresses, but the high tensile stresses can potentially cause a bond failure at the heat exchanger/skin joint. The consequences of such a failure are studied in the next example.

In order to illustrate the significance of viscoplastic phenomena, predictions of elastic theory are included in Figs.

9 and 10 for comparison (dashed line). The elastic computations were made with temperature-dependent elastic properties. The loss of stiffness due to the elevated temperatures for $0 < t < 0.5$ s accounts for the stress rolling over with an appearance of yielding. Generally, the elastic stresses are too high and, of course, since yielding does not occur, residual stresses are not predicted. Maximum deformations (not shown) predicted by the elastic analysis and viscoplastic analysis are about the same, approximately 0.001 in.

The two-dimensional character of the stress components σ_x and σ_y are shown in Figs. 11 and 12, respectively. The stress distributions are shown at three times, $t = 0.05$ s, 0.5 s, 1.2 s, in the response. The stresses at $t = 0.5$ s are residual stresses. Figure 13 shows contours of the principal plastic strains at $t = 0.5$ s. The contours show the relatively localized nature of the high stress gradients as well as the tensile and compressive regions. The significant residual stresses suggest the possibility of cumulative damage under repeated load cycles. This possibility needs further investigation.

The preceding analysis showed high tensile stresses in the heat exchanger fins and suggested the possibility of an aerodynamic skin/heat exchanger bond failure. To simulate such a possibility, the analysis was repeated but with the fins given greatly reduced material properties for a width of 0.30 in. under the high localized heating. Two results of this analysis are shown in Figs. 14 and 15. Since the fins can no longer support tensile stress, the internal coolant pressure causes substantial local deformation of the aerodynamic skin. Figure 14 shows the deformed structure at $t = 0.5$ s. The deformations, shown unmagnified, represent a significant permanent displacement. This result can be seen in Fig. 15, which compares displacement histories for the undamaged and damaged structure. For the damaged heat exchanger case, a residual permanent deformation of 0.007 in. is introduced by the thermal loading.

The maximum deformation induced by the fin damage depends strongly on the width of the damaged region. Increasing

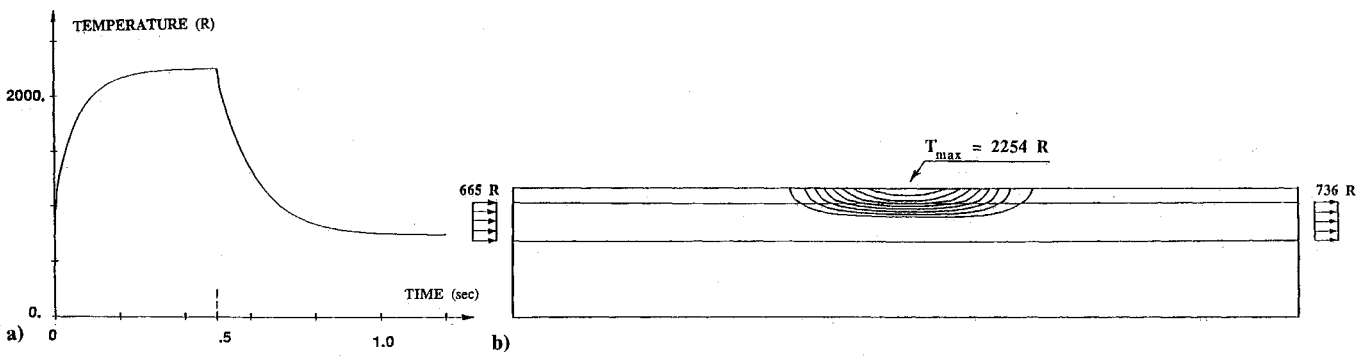

Fig. 8 Thermal response of two-dimensional model: a) temperature history at $x = 0.5$ in., $y = 0$; and b) temperature contours at $t = 0.5$ s.

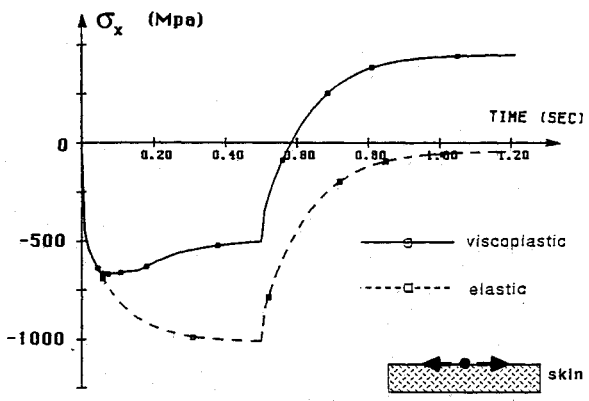

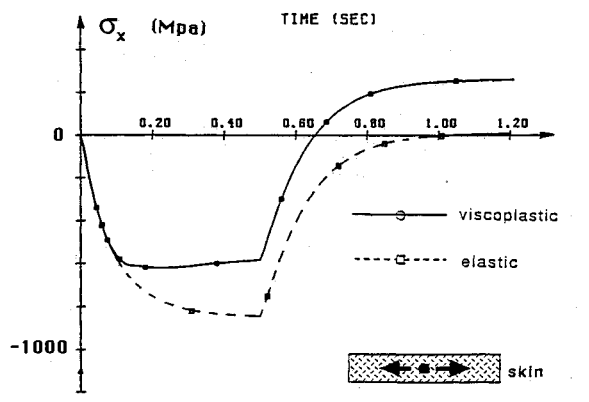

Fig. 9 Viscoplastic and elastic stress histories in aerodynamic skin for two-dimensional model.

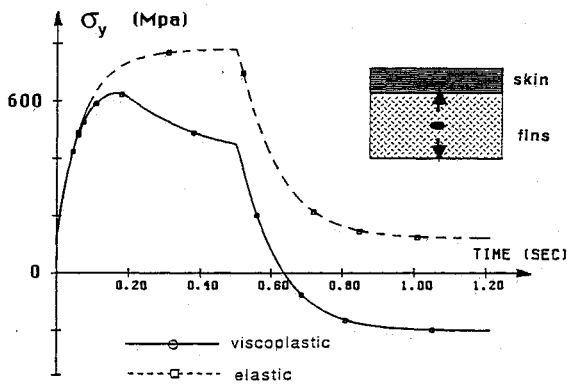

Fig. 10 Viscoplastic and elastic stress history in heat exchanger fins for two-dimensional model.

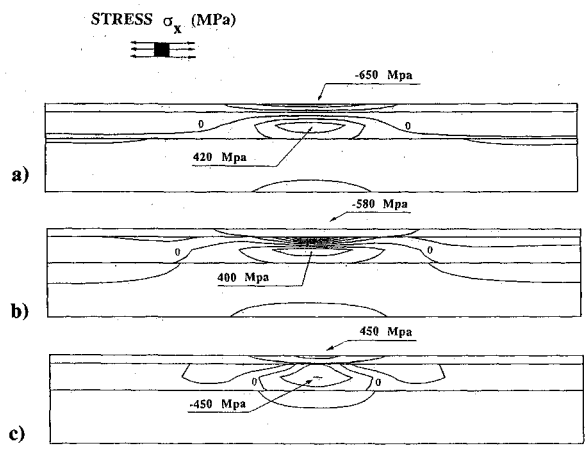

Fig. 11 Contours of σ_x stress in two-dimensional model: a) $t = 0.05$ s; b) $t = 0.5$ s; and c) $t = 1.2$ s.

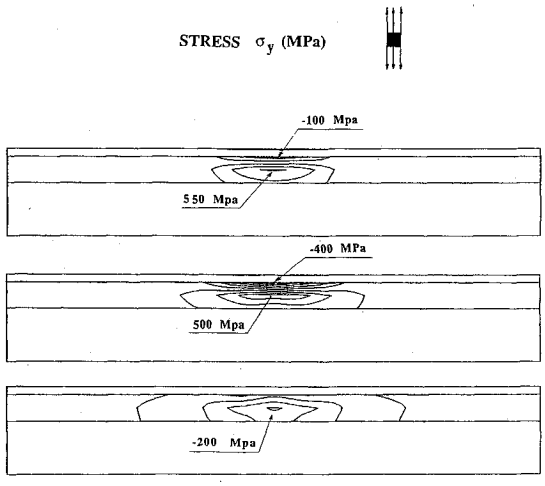

Fig. 12 Contours of σ_y stress in two-dimensional model: a) $t = 0.05$ s; b) $t = 0.5$ s; and c) $t = 1.2$ s.

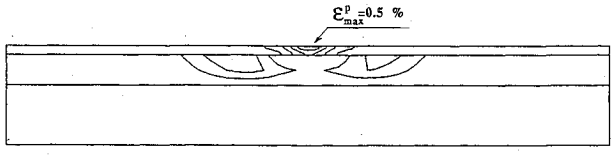

Fig. 13 Principal plastic strain in two-dimensional model at $t = 0.5$ s.

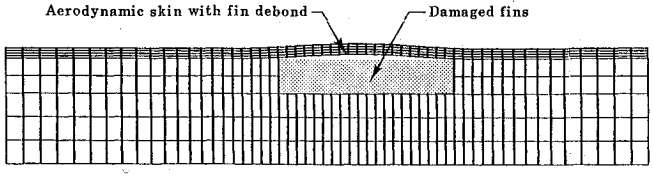

Fig. 14 Maximum deformation of structure ($t = 0.5$ s) with damaged heat exchanger fins; deformation is shown to scale.

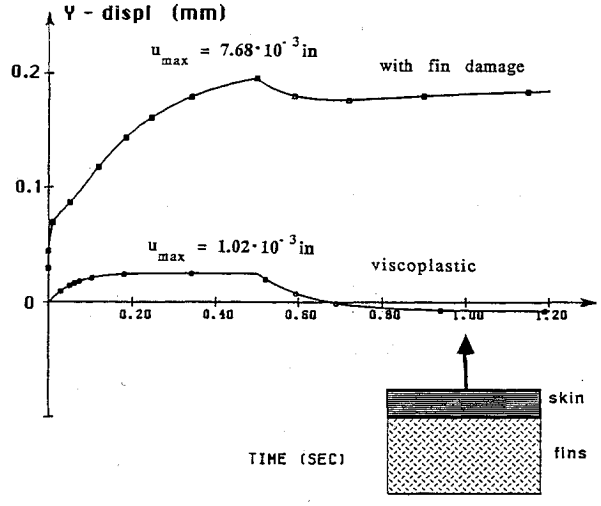

Fig. 15 Viscoplastic deformation of aerodynamic skin for undamaged and damaged heat exchanger fins.

the width of the damaged region by a small amount will substantially increase the deformation. The analysis of these large deformations requires that the present formulation be modified to account for large deformation effects.

A possible consequence of this permanent deformation is to cause a disturbance of the external flow. Protuberances into high speed flows can cause significant local augmentation of the aerodynamic heating. Thus, the significant permanent deformation introduced by a fin bond failure is likely to cause a complex flow-thermal-structural interaction.

Concluding Remarks

A thermoviscoplastic computational method for hypersonic structures subjected to severe local heating is presented. The method employs the Bodner-Partom unified viscoplastic constitutive model implemented in a finite element approach for quasistatic thermal-structural analysis. A variable time step algorithm is used to provide an efficient solution scheme for the stiff ordinary differential equation that characterizes the evolution of the internal state variables.

An analysis of a simplified model of a one-dimensional convectively cooled structure shows the basic features of the thermoviscoplastic response and demonstrates the substantial computer time savings as well as the reliability of the variable time step algorithm. An analysis of a two-dimensional model of a realistic convectively cooled structure provided more detailed understanding of the thermal structural behavior. The coolant flow dominates the thermal response providing a relatively short thermal transient. Under intense heating, significant local plasticity occurs in the aerodynamic skin, but the primary structure remains undamaged. Heat exchanger fins experience high tensile stresses and both the aerodynamic skin and heat exchanger fins have significant residual stresses. An analysis of an aerodynamic skin/heat exchanger fin bond failure showed that the aerodynamic skin would experience significant local plastic deformation due to the internal coolant passage pressure. The local deformation is pronounced enough to disturb the external aerodynamic flow and introduce a complex flow-thermal-structural interaction.

The thermoviscoplastic analysis of convectively cooled hypersonic structures under intense local heating shows the important role that such analyses can make in understanding complex transient inelastic structural behavior at elevated temperatures.

Appendix: Thermal-Structural Data

Thermal Data

1) Skin, heat exchanger fins and primary structure

$$\rho = 0.283 \text{ lb}_m/\text{in.}^3$$

Table A1 Temperature dependent conductivity and specific heat

T, °R	K, BTU/in. − sR	C_p, BTU/lb$_m$ − R
0	1.23×10^{-4}	0.12
500	1.8×10^{-4}	0.135
1500	3.25×10^{-4}	0.177
3000	6.0×10^{-4}	0.26

2) Coolant

$$\dot{m} = 7.17 \times 10^{-3} \text{ lb}_m/\text{s}$$
$$C_p = 3.48 \text{ BTU/lb}_m - \text{R}$$
$$T_0 = 665 \text{ R}$$
$$h = 6.2 \times 10^{-3} \text{ BTU/s} - \text{in.}^2 - \text{R}$$

3) Surface convection

$$T_\infty = 5345 \text{ R}$$
$$h = 6.0 \times 10^{-5} \text{ BTU/s} - \text{in.}^2 - \text{R}$$

Additional h at time $0 \le t \le 0.5$ s:

$$0 \le x < 0.375: \quad h_{add} = 0$$
$$0.375 \le x \le 0.625: \quad h_{add} = 3.0 \times 10^{-3} \cos \frac{(x - 0.15)}{0.05} \frac{\pi}{2}$$
$$0.625 < x \le 1.0: \quad h_{add} = 0$$

4) Surface radiation

$$\sigma = 3.30633 \times 10^{-5}\ \text{BTU/s} - \text{in.}^2 - \text{R}^4$$
$$\epsilon = 0.8$$
$$\alpha = 0.8$$

Structural Data (superalloy *B* 1900 + *Hf*)

1) Temperature-independent constants

$$D_0 = 1.0 \times 10^4\ \text{s}^{-1}$$
$$Z_1 = 3000\ \text{MPa}$$
$$Z_3 = 1150\ \text{MPa}$$
$$r_1 = 2$$
$$r_2 = 2$$
$$m_1 = 0.270\ \text{MPa}^{-1}$$
$$m_2 = 0$$

2) Temperature-dependent parameters

T	[°C]	≤760	871	982	1093
n		1.055	1.03	0.850	0.70
$Z_2 = Z_0$	[MPa]	2700	2400	1900	1200
A_1	[s^{-1}]	0	0.0055	0.02	0.25
A_2	[s^{-1}]	0	0	0	0

3) Elastic constants

$$E = 1.987 \times 16.78T - 0.1034T^2 + 1.143 \times 10^{-5}T^3\ \text{[MPa]}$$

$$G = 8.650 \times 10^4 - 17.58T + 0.02321T^2 - 3.464 \times 10^{-5}T^3\ \text{[MPa]}$$

(with temperature in °C)

4) Thermal expansion coefficient

T, °C	α, [1/°C] 10^{-5}
0	1.15
200	1.34
400	1.36
600	1.41
800	1.54
1000	1.60
1200	1.66

Acknowledgment

The authors are pleased to acknowledge the support of the Air Force Office of Scientific Research.

References

[1]Wieting, A. R., and Holden, M.S., "Experimental Study of Shock Wave Interference Heating on a Cylindrical Leading Edge," AIAA Paper 87-1511, June 1987.

[2]Dechaumphai, P., Thornton, E. A., and Wieting, A. R., "Flow-Thermal-Structural Study of Aerodynamically Heated Leading Edges," *Journal of Spacecraft and Rockets*, Vol. 26, No. 4, 1989, pp. 201–209.

[3]Polesky, S., Dechaumphai, P., Glass, C. E., and Pandy, A. K., "Three-Dimensional Thermal Structural Analysis of a Swept Cowl Leading Edge Subjected to Skew Shock-Shock Interference Heating," AIAA Paper 90-1710, June 1990.

[4]Melis, M. W., and Gladden, H. J., "Thermostructural Analysis with Experimental Verification in a High Heat Flux Facility of a Simulated Cowl Lip," AIAA Paper 88-2222, April 1988.

[5]Miller, A. K., *Unified Constitutive Equations for Creep and Plasticity*, Elsevier Applied Science, New York, 1987.

[6]Chan, K. S., Lindholm, U.S., Bodner, S. R., Hill, J. R., Weber, R. M., and Meyer, T. G., "Constitutive Modeling for Isotropic Materials (HOST)," NASA CR-179522, Aug. 1986.

[7]Chan, K. S., Lindholm, U.S., and Bodner, S. R., "Constitutive Modeling for Isotropic Materials (HOST)," NASA CR-182132, June 1988.

[8]Newman, M., Zaphir, Z., and Bodner, S. R., "Finite Element Analysis for Time-Dependent Inelastic Material Behavior," *Computers and Structures*, Vol. 6, 1976, pp. 157–162.

[9]Kaufman, A., Laflen, J. H., and Lindholm, U.S., "Unified Constitutive Material Models for Nonlinear Finite-Element Structural Analysis," AIAA Paper 85-1418, July 1985.

[10]Moreno, V., and Jordan, E. H., "Prediction of Material Thermomechanical Response With a Unified Viscoplastic Constitutive Model," *International Journal of Plasticity*, Vol. 2, March 1986, pp. 223–245.

[11]Bass, J. M., "Numerical Implementation of Constitutive Models in Rate-Dependent Plasticity," Ph.D Dissertation, University of Texas, Austin, TX, 1985.

[12]Bass, J. M., and Oden, J. T., "Adaptive Finite Element Methods for a Class of Evolution Problems in Viscoplasticity," *International Journal of Engineering Science*, Vol. 25, No. 6, 1987, pp. 623–653.

[13]Bass, J. M., and Oden, J. T., "Numerical Solution of the Evolution Equations of Damage and Rate-Dependent Plasticity," *International Journal of Engineering Science*, Vol. 26, No. 7, 1988, pp. 713–740.

[14]Chang, H. T., and Allen, D. H., "Analysis of Viscoplastic Plates Subjected to Rapid External Heating," AIAA Paper 88-2422, April 1988.

[15]Huebner, K. H., and Thornton, E. A., *The Finite Element Method for Engineers*, 2nd ed., Wiley, New York, 1982.

[16]Thornton, E. A., and Wieting, A. R., "Finite Element Methodology for Transient Conduction/Forced Convection Thermal Analysis," *Progress in Astronautics and Aeronautics: Heat Transfer, Thermal Control and Heat Pipes*, Vol. 70, edited by W. B. Olstad, AIAA, New York, 1980, pp. 77–103.

[17]Kumar, V., Morjaria, M., and Mukherjee, S., "Numerical Integration of Some Constitutive Models of Inelastic Deformation" *Journal of Engineering Materials and Technology*, Vol. 102, Jan. 1980, pp. 92–96.